Ab Initio Molecular Dynamics Study of Heterogeneous Oxidation of Graphite by Means of Gas-Phase Nitric Acid§

Antonio Rodríguez-Fortea,*,† Marcella Iannuzzi,‡ and Michele Parrinello*

Computational Science, Department of Chemistry and Applied Biosciences, ETH Zurich, USI Campus, Via Giuseppe Buffi 13, CH-6904 Lugano, Switzerland

Received: May 13, 2005; In Final Form: August 4, 2005

The interaction between gas-phase nitric acid and the graphite surface is taken as a simple model of interactions occurring at the surface of atmospheric soot particles. In particular, we study the heterogeneous processes that lead to the dissociation of the nitric acid and the production of nitrous acid. The atomistic details of the reaction mechanisms are reproduced by use of the new metadynamics method. The binding interactions of the HNO_3 molecule and its fragments with the graphite surface are calculated, and the role of the surface in catalyzing the reaction is taken into account. From the reactive trajectory generated by the metadynamics, it is seen that the path goes through several different intermediate states. We analyze in detail the electronic structures and spin density distributions of the relevant products and report on the mechanisms and the main features of the transition regions relative to all the activated processes observed.

Introduction

Condensed particulate matter is ubiquitous in the lower atmosphere. Elemental-carbon-soot particles are produced during incomplete combustion processes and consist mainly of coagulated graphitic layers with condensed polycyclic aromatic hydrocarbon (PAH) superstructures.[1−4] Soot may have an influence on the chemical composition of the atmosphere by facilitating reactions that are slow or impossible in the gas phase. It has been observed that soot particles play an important role in the reduction processes of oxidized species that otherwise would not occur in the earth's oxidizing atmosphere.[5−14] The extent to which one soot particle can be involved in such processes depends on its ability to recover the initial surface characteristics after it has been oxidized.

Nitrogen oxides also play a very important role in atmospheric processes. The most important ones are nitrogen monoxide, NO, and nitrogen dioxide, NO_2, usually indicated as NO_x. These species can be removed from the atmosphere by the formation of nitric acid, HNO_3, which is subsequently deposited by either a dry or a wet process. However, it has been reported that the $[HNO_3]/[NO_2]$ ratios measured in the free troposphere are significantly lower than the values predicted from atmospheric theoretical models. On the basis of experimental results, it has been proposed that HNO_3-to-NO_2 recycling processes (known as renoxification) can justify this discrepancy.[6,8,15,16] An example of such renoxification processes is the heterogeneous reduction of HNO_3 on soot-particle surfaces.

$$HNO_3 \xrightarrow{\text{soot}} NO,\ NO_2 \qquad (1)$$

If confirmed, high rates of reactions of this kind would have a direct impact on the ozone production and destruction processes.[6,11] Another interesting point is that, although fresh soot from a combustion source is hydrophobic, these types of reactions render soot particles hygroscopic, which would result in an enhancement of water deposition with the consequent formation of potential cloud-condensation nuclei.[14,17]

Despite the large amount of experimental work done in this field, there are almost no theoretical studies tackling these problems. The main difficulty arises in modeling the soot; it is known that the bulk structure is made up of an irregular agglomeration of graphite layers,[3] but the surface structure remains unclear. The most common choice is to model the oxidized soot surface by introducing oxygen-containing functionalities (like carboxylic acids, ketones, and ethers) in molecular PAH-type systems.[18−25] In recent work by Ghigo et al.,[20] either a PAH-type system or a periodic graphene layer (with and without defects) is used to study the interactions of small inorganic oxidant species with sootlike surfaces.

Our aim is to shed some light on the heterogeneous processes that lead to the dissociation of HNO_3 molecules in the gas phase. Although the oxidation of graphite by nitric acid in water solutions is well-known and has been extensively studied,[26] the role of the carbon layer during the dissociation in the gas phase is still not clear and there are no data on the corresponding activation energies required for the functionalization (oxidation) of the graphite surface. Here, we investigate the effect of carbon particles on the HNO_3-dissociation process by comparing the reaction mechanisms observed in a vacuum to those observed in the presence of a graphite layer. Our model of soot, that is, a two-dimensional graphene layer, lacks border effects or defects that provide the surfaces with an enhanced reactivity toward the atmospheric species. Nevertheless, we are interested here in scrutinizing the reactivity of the exposed basal planes of an undefective graphitic nature that are in the soot particles.

As a result of the high activation energies and the complexity of the reaction pathway that involves several intermediate metastable states, the standard ab initio molecular dynamics (MD) techniques would not be able to reconstruct the reactive trajectory in an affordable simulation time. To this end, we apply

§ Part of the special issue "Michael L. Klein Festschrift".

* To whom correspondence should be addressed. E-mail: antonio.rodriguezf@urv.net, parrinello@phys.chem.ethz.ch.-

† Current address: Departament de Química Física i Inorgànica, Universitat Rovira i Virgili, C/Marcel·lí Domingo s/n, 43007 Tarragona, Spain.

‡ Current address: Physikalisch-Chemisches Institut, Universität Zürich, Winterthurerstr. 190, CH-8057 Zurich, Switzerland.

10.1021/jp052526h CCC: $33.50
Published on Web 09/10/2005

the metadynamics method in its extended Lagrangian form, as implemented in the Car−Parrinello MD (CPMD) package.[27,28] This technique can efficiently reproduce the most probable reaction pathways, clearing high barriers and providing quite an accurate picture of the free-energy profile. Several examples of the successful employment of metadynamics are reported in refs 27 and 29−33.

The paper is organized as follows: In Computational Methodology, we give some technical details about our computational approach and discuss the metadynamics technique in more detail. In Results and Discussion, the dissociation reaction of the nitric acid is thoroughly investigated. First, we report on the calculation of the dissociation energy in the gas phase and compare our results with previously published quantum-chemistry studies to validate our description of the electronic structure. In the remaining part of the section, we study the role of graphite during the dissociation. In this context, we also discuss the most relevant electronic and structural properties of the intermediate states and the activation energies involved in the process.

Computational Methodology

The results presented in this work are all obtained at the density functional level of theory (DFT). We use the CPMD-program package,[34] where the description of the electronic structure is based on the expansion of the valence wave functions into a plane wave (PW) basis set, supported by the pseudopotential (PP) approximation. In the MD simulations, the propagation of the wave functions is treated in the Car−Parrinello scheme by integrating the equations of motion derived from the extended Car−Parrinello Lagrangian.[35]

All the calculations are performed with the generalized gradient-corrected Becke−Lee−Yang−Parr (BLYP) exchange-correlation functional[36,37] in the spin unrestricted formalism. The interactions between electrons and ionic cores are described by the Martins−Troullier atomic norm-conserving PPs.[38] In the CPMD simulations, we use a time step of 0.12 fs and a fictitious electronic mass of 800 au. The temperature is controlled by rescaling the atomic velocities to keep the system at about 300 K. The reported geometry optimizations or transition state (TS) searches are performed with the pseudo Newton−Raphson method, where an empirical initial Hessian is progressively updated with the Broyden−Fletcher−Goldfarb−Shanno algorithm.[39,40] Within this scheme, given an initial geometry, the TS is defined as the closest saddle point on the potential energy surface (PES) and its structure is determined and optimized via the eigenvector-following procedure.[39] The calculations with atom-centered Gaussian functions have been performed with the Gaussian 98 (G98) package.[41]

As a result of the rather high computational costs, ab initio MD trajectories are in general restricted to a few picoseconds. Such a short time scale makes it impossible to observe the majority of the interesting processes that are in the class of rare events, like thermally activated reactions, conformational changes, phase transformations, and so forth. The metadynamics approach offers the possibility to go beyond these limits and to observe complex reaction mechanisms within an affordable simulation time. The metadynamics method is based on the assumption that the reaction pathway can be described in terms of a reduced number (N_α) of collective variables (CV), $S_\alpha(R_I)$ with $\alpha = 1, ..., n$, which are continuous and derivable functions of the atomic coordinates R_I. In other words, a dynamics in the space of these few CV should be able to reproduce the relevant features of the reaction mechanism, discarding the fast degrees of freedom that are not relevant. Therefore, the CV should be able to represent all those slow processes that cannot be properly sampled by a standard MD run and need to be activated. The metadynamics algorithm consists of the construction of a metadynamics trajectory in the space of the CV, in terms of the additional variables s_α. This metadynamics trajectory is coupled to the standard MD trajectory by the following extended Lagrangian

$$L = L_{CP} + \sum_\alpha \frac{1}{2} M_\alpha \dot{s}_\alpha^2 - \sum_\alpha \frac{1}{2} k_\alpha [S_\alpha(R_I) - s_\alpha]^2 - V(t,\vec{s})$$

where L_{CP} is the Car−Parrinello Lagrangian.[35] Each additional variable s_α is coupled to the actual value of $S_\alpha(R)$ of the CV through the harmonic potential $0.5\{k_\alpha[S_\alpha(R) - s_\alpha]^2\}$. The fictitious kinetic energy of the s_α is controlled by a velocity rescaling algorithm, whereas the M_α and k_α parameters determine, respectively, the frequency and the amplitude of the fluctuations of the s_α variables. The metadynamics trajectory is encouraged to explore thoroughly all the available configurations by the introduction of a repulsive, time-dependent potential $V(t,s)$. In the equations of motion of the s variables, two force contributions appear: one force is coming from the coupling potential $\phi_\alpha = k_\alpha[S_\alpha(R) - s_\alpha]$, which recalls the metadynamics trajectory toward the minimum of the basin of attraction, and the second force is from the repulsive potential $V(t,s)$, which, on the contrary, drives toward unvisited regions. Our choice for the history-dependent potential is a sum of Gaussian-like hills of the form

$$V(t,\vec{s}) = \sum_{t_i<t} W_i \exp\left[-\frac{(\vec{s} - \vec{s}^{\,i})^2}{2(\Delta s^\perp)^2}\right] \times \exp\left\{-\frac{[(\vec{s}^{\,i+1} - \vec{s}^{\,i})(\vec{s} - \vec{s}^{\,i})]^2}{2(\Delta s_i^{||})^4}\right\}$$

where V is modified at each metadynamics step (50−100 MD steps) by the addition of a new hill located in the region that has just been explored by the trajectory. The size of the ith hill is determined by $\Delta s_i^{||}$, which corresponds to the displacement along the metadynamics trajectory since the last metadynamics step, and by the transversal width $\Delta s_i^\perp$, which is usually kept constant along the whole run. For an efficient sampling, $\Delta s_i^\perp$ should be of the same magnitude as the typical fluctuations of the CV in equilibrium conditions. The hill's height, W_i, should not be larger than a few percentages of the smallest barriers that have to be estimated. It can be tuned at each step to obtain a good balance among all the force contributions acting on the metadynamics trajectory.

By the progressive accumulation of hills, the energy well is filled layer by layer, and the metadynamics trajectory, as well as the MD trajectory thanks to the coupling, is forced farther and farther from the initial equilibrium state until it eventually finds the lowest TS and the new, unexplored basins of attraction.

An appropriate choice of parameters and accumulation rates results in a metadynamics trajectory that lies on the minimum-energy pathway. In these conditions, it has been shown that the time-dependent potential converges to the free-energy surface in the space of the selected CV.

$$\lim_{t\to\infty} V(t,\vec{s}) = -F(\vec{s}) + \text{constant}$$

All the parameters are obviously system-dependent, and they strongly affect the efficiency in escaping from the minima as well as the accuracy in reconstructing the underlying free-energy surface.

An important condition for the metadynamics to give correct results is that the selected CV include implicitly all the relevant modes that need to be activated and can be distinguished among all the intermediate states that characterize the reaction path. However, the dimensionality of the CV space (n) cannot be arbitrarily large, because the volume to be filled by the added hills grows as Δs^n. In practice, a choice of more than six CV would not provide an efficient sampling. Here, we employ $n = 3$.

Technical Details

Simulations of surfaces are typically done using rather thick slabs of atomic layers to model correctly the interaction of the surface regions with a semi-infinite bulk. However, as a result of the deficiencies of DFT in reproducing the weak, van der Waals interactions between the graphite layers,[42−44] additional constraints should be imposed to maintain the experimental interlayer distance in a graphite slab. On the other hand, because the interactions are so weak, the processes occurring at the surface are not much affected by the presence of deeper layers; that is, the reactive PES remains the same with slight changes in relative energies. We have checked that the introduction of a second layer in the model provides relative energies that differ by less than 2 kcal/mol. As a consequence, we can safely model the graphite surface by one single graphene layer, as was already done in previous computational studies.[20]

Our typical simulation system is a graphite layer plus one or more molecules on top of it. By using periodic boundary conditions (PBC) in the three dimensions of space, the cell box has to be chosen large enough to avoid any relevant interaction between the molecules and their periodic images, as well as with the periodic image of the graphite layer. Test calculations demonstrate that box sides $a = 18.7$, $b = 16.2$, and $c = 20.0$ au are required for a graphite layer of 32 C atoms in the xy plane and one HNO_3 molecule.

One CV often used in the metadynamics runs is the coordination number (CN) of one atom or group of atoms, A, with respect to a second atom or group of atoms, B.[27,45] The CN provides information on the interaction pattern characterizing the actual atomic configuration, and it is a rather general order parameter that reduces the risks of biasing the reaction in a predetermined direction, as often happens when using bond lengths or angles. The analytical expression that we use for the CN is

$$C_{AB} = \sum_{i=1}^{N_A} \frac{1}{N_A} \left[\sum_{j=1}^{N_B} \frac{1 - (r_{ij}/d_{AB})^p}{1 - (r_{ij}/d_{AB})^q} \right], \quad \text{with } q > p$$

where N_A and N_B are the number of atoms in groups A and B, respectively, and d_{AB} is a reference distance that determines the presence of A−B interactions. The choice of d_{AB} and of the exponents p and q determines the decay behavior of the C_{AB} function. In the present work, we chose the values $p = 6$ and $q = 10$.

Results and Discussion

1. Dissociation of HNO_3 in the Gas Phase. First of all, we consider the dissociation reaction of the nitric acid molecule into the NO_2 and OH radicals in the gas phase (process 2).

$$HNO_3 \rightarrow NO_2 + OH \quad (2)$$

This process and its inverse reaction have been extensively investigated from both experimental[46,48,49] and theoretical points of view.[47,50−52] In Table 1, we report the reaction energies for the formation of HNO_3 from the reactants NO_2 and OH, as calculated at different levels of theory.

All-electron DFT calculations reproduce fairly well the experimental binding energy and the G2 level of theory results. However, when the PW basis set and the PP approximation are used, the nonlinear core correction (NLCC)[53] and a very high-energy cutoff are required to achieve the same accuracy as all-electron calculations. Without the NLCC, the binding energy is underestimated by about 10% (5 kcal/mol), irrespective of the type of PP and the PW cutoff, as a result of an overestimation of the radical ground-state energy.[54,55] Namely, the spin-polarized states of the dissociated molecule are poorly described by a simple PP approximation with frozen core electronic structure. On the other hand, the introduction of core polarization makes the PP much harder so that we need a rather high cutoff for an appropriate expansion of the wave functions. Because the shape of the PES is not altered by the introduction of the NLCC, the optimized geometries obtained at the all-electron level and by the PW−PP approximation, with or without NLCC, are essentially the same. In the following, we use the computationally demanding NLCC and high PW cutoff only to calculate accurate energy differences between stationary states on the PES. Otherwise, all the MD runs and geometry optimizations reported in this work are performed with simple norm-conserving PP and with an energy cutoff of 70 Ry.

To further assess the quality of the barriers found with the BLYP functional in these types of systems, we have analyzed a couple of gas-phase reactions in which the HNO_3 molecule and the C−C bonds are involved. In the first one, we have computed the barrier for the reaction between HNO_3 and ethylene at the MP2 and DFT (B3LYP and BLYP) levels. We observe (see Appendix) that the B3LYP and MP2 results are the same (within 1 kcal/mol) and that the BLYP functional, regardless of the set of basis functions employed (PW or atom-centered Gaussians), underestimates somewhat the barrier (around 20%). We have also examined the gas-phase reaction between the HNO_3 and benzene molecules, a system that is very similar to the one analyzed in the present work. We have found a TS with a considerable open-shell biradical structure (such as the one found for the oxidation of graphite). In these cases, the second-order perturbation theory, based on a single-determinant wave function, is not appropriate to describe the TS, and a multiconfigurational (MC) method is needed to obtain an accurate estimation of the barrier. On the other hand, it has been shown that this type of biradical system is well-described at the B3LYP level.[56−59] We, therefore, compare the BLYP results to those of the B3LYP while avoiding the computationally expensive MC methods. We observe (see Appendix) here as well that the BLYP functional underestimates around 20% of the barrier compared to the B3LYP functional. Thereby, we have to be aware of the fact that the BLYP functional employed here underestimates, somewhat, the reaction barriers in these types of systems.

2. Oxidation of Graphite. *2.a. Interaction of the HNO_3 Molecule with the Graphite Surface.* The position of a HNO_3 molecule over the graphite surface can be described by the distance of its center of mass along the normal axis to the surface and the angle between the surface plane and the molecular plane, defined as the plane containing the N atom and the two O atoms not bonded to H.

TABLE 1: Binding Energies (at 0 K and without Zero-Point Energy Corrections) of HNO_3 with Respect to the Dissociation into OH and NO_2 Radicals at Different Levels of Theory[a]

level of theory	ΔE (kcal/mol)
G2[b]	−53.0
B3LYP/6-311G (d,p)	−47.7
BLYP/6-311G (d,p)	−48.8
BLYP/6-311++G (d,p)	−47.8
BLYP/6-311++G (2df,2pd)	−49.9
BLYP/PW (MT NLCC, 500 Ry)	−49.6
BLYP/PW (MT NLCC, 400 Ry)	−49.2
BLYP/PW (MT, 110 Ry)	−44.8
BLYP/PW (MT, 70 Ry)	−44.5
BLYP/PW (MT, 50 Ry)	−43.9
BLYP/PW (SG, 400 Ry)	−44.7
BLYP/PW (SG, 300 Ry)	−44.6

[a] MT stands for Martins−Troullier, SG stands for Goedecker PPs, and NLCC stands for nonlinear core correction. The counterpoise correction is included to assess the basis-set superposition error when atom-centered basis sets are employed. The experimental dissociation energy is 47.7 kcal/mol.[46] [b] From the value found in ref 47, which corresponds to a modified Gaussian 2 method, we have subtracted the zero-point energy and added the counterpoise correction.

We used either geometry optimization or metadynamics to explore all the positions of the molecule corresponding to minimum energies. As expected, the interactions between the graphite layer and one molecule turn out to be rather weak. The DFT minimum-energy distance between the molecule and the layer remains larger than 4 Å, irrespective of the orientation of the molecule. The inclusion of the dispersion energy might improve the description of the equilibrium geometry and the stability of this complex. However, this is generally done by empirical corrections that are system-dependent.[60−63]

2.b. Metadynamics of the Oxidation Process. Although it has been reported that nitric acid solutions are able to oxidize the graphite surface,[26] the mechanism of oxidation by HNO_3 in the gas phase has not been investigated in detail. Because such a process requires rather high activation energies, we are very unlikely to observe it in standard MD simulation unless the temperature and gas pressure are increased to extreme values, which would surely change the physics of the reaction. Therefore, we resort to the metadynamics technique to be able to reproduce the reaction path and estimate the energy barriers involved.

Because the weakest N−O bond in the HNO_3 molecule is the one with the hydroxyl O atom (1.410 Å in contrast to 1.213 and 1.198 for the cis and the trans O atoms, respectively),[64] it is reasonable to expect the oxidation process to occur through the dissociation of the hydroxyl group. Under this assumption, we take as the CV the N−OH distance, the distance between the hydroxyl O atom and the graphite surface, and the distance between the remaining NO_2 group and the surface, taking as a reference point the geometrical center of the three atomic positions. The third CV is useful to control the position of the molecule over the surface before the reaction but also to sample the interactions of the NO_2 radical with the C atoms once the dissociation is complete. As PBC are always used in all three dimensions, a stiff constraining potential is added to prevent the molecules from going too far in the *z* direction, where they might interact with the periodic image. This constraint keeps the molecules within 4 Å of the layer. The confinement of the HNO_3 molecule and its fragments in the region close to the surface offers an additional advantage in the metadynamics simulations. Indeed, it restricts the CV space that has to be explored by neglecting those regions of little interest that are far from the surface where the energy profile is flat.

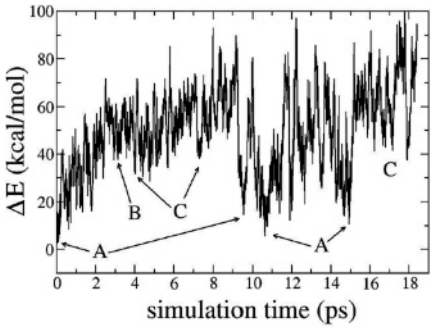

Figure 1. Evolution of the KS energy along the trajectory of the metadynamics run. The capital letters A, B, and C label the regions and energy values corresponding to the three local minima visited during the trajectory.

Here, we give a qualitative description of all the events that have been observed during an 18-ps metadynamics run.[65] More details about the electronic structures of the intermediate states, the energy barriers, and the mechanisms are provided in the following subsections. Our starting structure is the minimum-energy configuration of the HNO_3−graphite system, as obtained by optimization, where the molecule is at about 4 Å from the graphite surface. From the beginning of the exploration, the metadynamics time-dependent potential induces large variations in the HNO_3−graphite distance, forcing the molecule to visit high-energy states that are typically very close to the surface. Fluctuations of 30 kcal/mol are observed in the Kohn−Sham (KS) energy (Figure 1), as calculated along the trajectory that corresponds to changes in the HNO_3−graphite distance from 4 to about 3 Å.

After 2 ps of metadynamics, one of these fluctuations leads to the dissociation of the nitric acid and the formation of the two radicals NO_2 and OH. The OH radical is immediately attracted by the graphite surface where it binds to one of the C atoms (process 3).

$$HNO_3 + \text{graphite} \rightarrow NO_2 + \text{graphite}-OH \qquad (3)$$

The NO_2 radical, instead, moves farther from the surface as shown in Figure 2a. Along the energy profile in Figure 1, the letter B labels the region corresponding to this intermediate configuration. A first estimation of the energy barrier for this process can be inferred from the fluctuation of the KS energy just before the dissociation, and it is about 35−40 kcal/mol. Immediately after the dissociation, the biradical system is further stabilized by the transfer of the H atom from the hydroxyl radical to the NO_2 group resulting in the formation of nitrous acid HNO_2 (process 4). Free from the H atom, the O atom on the surface prefers an epoxide configuration; that is, it forms two bonds with two neighboring C atoms, as shown in Figure 2b. Along the energy profile, C indicates the regions corresponding to this closed-shell configuration.

$$NO_2 + \text{graphite}-OH \rightarrow HNO_2 + \text{graphite}-O \qquad (4)$$

The two possible adsorbates on graphite, O and OH, have already been observed in previous experimental[66] and theoretical studies.[20,67,68] In particular, the adsorption of oxygen on graphite and on single-walled carbon nanotubes has been investigated in a recent DFT/PW study where the formation of a highly stable spin-singlet epoxide structure was observed.[68]

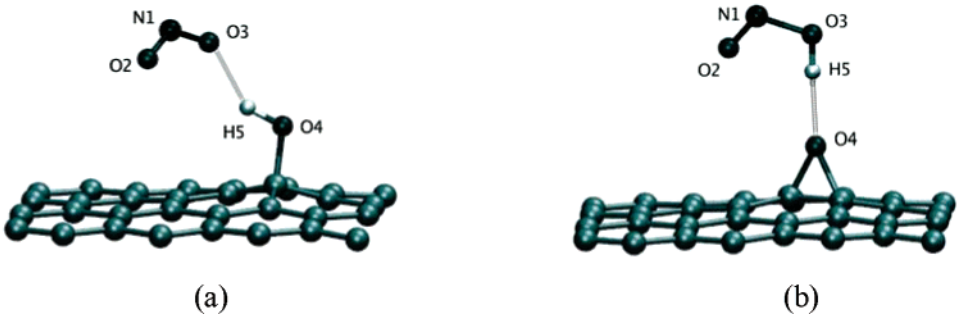

Figure 2. (a) Geometry of the intermediate B, hydroxylated surface. (b) Geometry of the intermediate C, surface with an epoxide-like group.

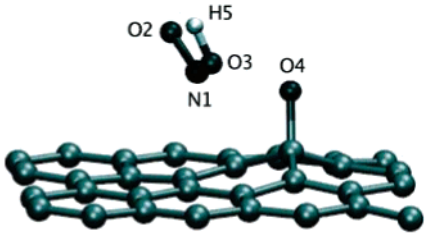

Figure 3. Sketch of the TS in the hopping process of the O atom over the graphite surface.

After the first dissociation, the H atom is exchanged several times between the O atom on the surface and the NO_2 group, while the molecular fragment fluctuates back and forth over the surface. When the O atom is free from the H atom and forms the epoxide, it also migrates over the surface by breaking one of the two bonds of the epoxide and binding to a new C atom on the opposite side of the fixed bond (Figure 3).

At about 9 ps, we observe the back transfer of the O atom from the surface to the HNO_2 molecule (process 5; about 45 kcal/mol barrier)

$$HNO_2 + \text{graphite}-O \rightarrow HNO_3 + \text{graphite} \qquad (5)$$

and the system falls back into the initial reactant state.

Because, after this first recrossing, the metadynamics trajectory has already visited the lowest energy reaction path, the further prolongation of the metadynamics run can drive the system along alternative pathways, if available, possibly through a TS higher in energy.

Eventually, a new graphite oxidation process is observed, but this time, the attacking O atom is not the hydroxyl O atom. In fact, this is a one-step reaction that is exactly the inverse of process 5. This one-step process requires a much higher activation energy with respect to the two-step reaction (HNO_3 dissociation and subsequent H transfer). The energy barrier estimated from the energy profile along the trajectory is about 75 kcal/mol.

2.c. Characterization of the Minima. In this and the following sections, we characterize in more detail the most interesting stationary points (intermediates and TS) observed during the metadynamics run described. The energy differences and the activation energies are accurately estimated using the NLCC for the radical states.

The energy differences have been calculated on the optimized structures of the minima A (HNO_3 + graphite), B (NO_2 + graphite−OH), and C (HNO_2 + graphite−O) encountered along the first reaction path. The results obtained from these calculations show that B and C are quasidegenerated, whereas A is much more stable (see Table 2).

As already mentioned, in the A configuration, the minimum energy is obtained when the HNO_3 molecule is placed more than 4 Å from the surface. Also, the minimum-energy distance of the NO_2 radical (B) from the surface is about 4 Å. However, in this case, the molecule interacts with the surface via the formation of a H bond between one of its O atoms and the H atom of the adsorbed hydroxyl group (see Figure 2a). The H-bond length is 1.93 Å with a binding energy of 3.9 kcal/mol. The unpaired electron of the adsorbed OH is transferred to the surface itself. The C′ atom binding the OH shows an sp^3 hybridization, with pyramidalization angles (CC′O) of 104.8°. The average C−C′ distance is 1.51 Å; that is, it is longer than the characteristic C−C distance in a nonfunctionalized graphite layer (1.43 Å). The C′−O distance is 1.51 Å, which is also longer than the typical C−O single bond length (1.43 Å for methanol, CH_3OH).

TABLE 2: Relative Energies, E_{rel}, and Type of the Electronic Shell for Minima A, B, and C[a]

minimum	E_{rel} (kcal/mol)	electronic shell
A	0.0	closed
B	31.7	open
C	29.8	closed

[a] The energy values refer to the optimized geometries.

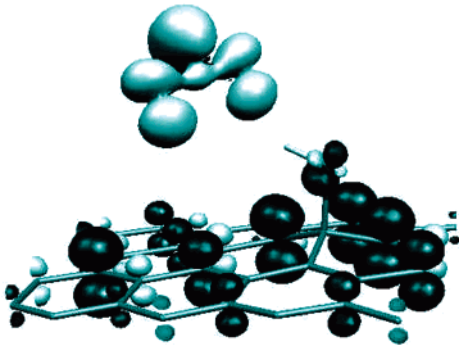

Figure 4. Representation of the isodensity surface (0.003 $e^-/bohr^3$) of the spin density for the lowest-energy open-shell singlet state of minimum B.

In Figure 4, the black and white isosurfaces reproduce the spin-up and spin-down densities in the optimized B state. The spin distribution on the NO_2 radical is delocalized over the three atoms as a result of the delocalized nature of the molecular orbital that bears the unpaired electron. The delocalization of the spin density on the graphite layer is a consequence of the characteristic π-electronic system. The coexistence of the spin delocalization and the spin polarization mechanisms induces a regular pattern in the distribution.[69,70] Namely, the π band where the unpaired electron is accommodated is delocalized over the odd neighbors of the C′ atom (first, third, etc.). On the other hand, the presence of the unpaired electron in the valence band polarizes the electron pairs in the bonds, and a spin density is also induced on the even neighbors of C′ (second, fourth, etc.) but of the opposite sign.

Also, the optimized geometry of the C intermediate is characterized by a weak interaction between the molecule and the O atom on the surface. The H atom, which now is on the molecule, forms an H bond of 2.00 Å with the epoxide O atom. The epoxide C′−O bond lengths are 1.52 Å. The C′−C′ distance is 1.50 Å; these two carbon atoms show a constrained sp^3 hybridization. The slight pyramidalization of the C′ atoms with respect to the three nearest C atoms on the layer is given by an angle of 356.2°.

2.d. Dissociation of the Nitric Acid Molecule. The first event observed in the metadynamics run described above is the dissociation of the nitric acid through the cleavage of the bond between the N and the hydroxyl O atom. Moreover, the energy profile calculated for this run shows that this step is also the rate-limiting event in the oxidation of graphite by nitric acid. However, for a better understanding of the role of graphite in the dissociation and for a more accurate evaluation of the activation energy involved, we carried out a second metadynamics run with different CV. In the first metadynamics, we focused our attention on the hydroxyl group, assuming that the N−OH bond is the one most likely to break in the dissociation event. The three CV selected for this second run, on the other hand, do not distinguish among the O atoms to not bias the reaction path towards a predetermined direction. The first CV is the CN of N with respect to the three O atoms, the second CV is the average CN of the O atoms with respect to all the C atoms, and the third CV is the CN of N with respect to all the C atoms. This last variable samples the interactions of the nitric acid, or its fragment NO_2, with the surface. As we are interested in studying the dissociation process near the graphite surface, once more we introduce a boundary potential on the second CV to keep the molecule within 3.2 Å of the surface. This restricts the metadynamics exploration only in the region of the CV space where there is a significant interaction between the molecule and the graphite. In this region, the graphite might play an active role in the reaction process if it stabilizes the early products of the dissociation by adsorbing one or more radicals. The restriction imposed by the boundary-potential model was a rather high partial pressure of the HNO_3 gas that could not be simulated other than by adding many more HNO_3 molecules and, thus, dramatically increasing the computational costs. The parameters used in this metadynamics run are described in ref 71.

Once more, in this second run, the first observed events (at about 9 ps) are the cleavage of the N−OH bond and the formation of the two radicals NO_2 and OH. The weakening of the N−OH interaction starts when the molecule is at about 2.6 Å from the surface. However, from this new trajectory, it is clearly seen that the OH−graphite interaction starts before the complete dissociation and affects the process. Thanks to this interaction, the activation energy for this process is lower than the one calculated for the dissociation in a vacuum. We performed a standard TS search, using as a starting structure a snapshot extracted from the reactive trajectory, in the region of the transfer of the OH. The TS obtained (TS1) has an electronic energy 36.7 kcal/mol higher than that of state A but 12.5 kcal/mol (25%) lower than the dissociation energy in the gas phase. This result supports the hypothesis that there is an important catalytic effect from the graphite. The C′···O distance is found to be 1.77 Å in the TS geometry, whereas the N···O distance is 2.34 Å. The C′ atom already shows a large amount of sp^3 hybridization and pyramidazilation, where the average of the C′−C distances is 1.47 Å and the sum of the three C−C′−C angles is 351.0°. The normal mode with the imaginary frequency corresponds to the displacement of the OH group between the N and C′ atoms [the N−O(H)−C′ angle in the TS1 structure is 163.5°; see Supporting Information].

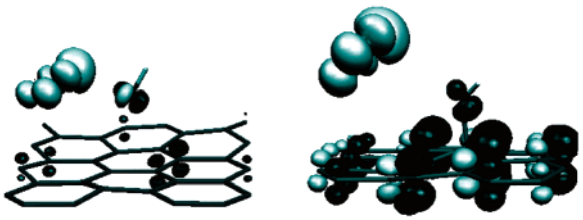

Figure 5. Representation of the isodensity surface (0.003 $e^-/bohr^3$) of the spin density of the lowest-energy open-shell singlet state at two points in the metadynamics trajectory. The incipient OH radical from the HNO_3 dissociation is stabilized by the electronic π system of the surface (left). When the C−O bond is formed, the delocalization of the spin density over the surface is more evident (right).

From the analysis of the spin density during the dissociation process, we observe that there is an interaction between the incipient radicals and the graphite surface that stabilizes the system. This interaction first appears when the N−OH distance is around 2.1 Å, whereas the O of the OH group is at about 2.5 Å from the closest C atom on the surface (Figure 5, left). As soon as the system moves forward from this transition region, the OH radical is definitively adsorbed at the surface, and its unpaired electron is delocalized on the graphite surface, as shown in Figure 5 (right).

2.e. Formation of Nitrous Acid (HONO) from the NO_2 Radical. In this section, we focus our attention on the H-transfer process from the OH adsorbed on the surface to the NO_2 radical. We take as our initial configuration the intermediate with the hydroxylated surface, as described in subsection 2.c. The reactant and product states of the H transfer are very close in energy (a 1.9 kcal/mol difference) even when the two electronic structures are substantially different. We go from an open-shell biradical system to the slightly more stable closed-shell system with the formation of the nitrous acid, HONO. HONO is an important trace gas in atmospheric chemistry because its photolysis significantly enhances the photo-oxidation processes in the early morning as a result of the rapid production of OH radicals.[7,12,72,73] However, the mechanism by which HONO is formed is not yet completely understood despite many scientific works that have been devoted to this subject.[7,9,10,12,73,74] Just before the H transfer, the metadynamics trajectory explores regions that are only 10 kcal/mol higher in energy with respect to the minima, which means that the energy barrier should be within this order of magnitude. The TS search, started from a trajectory snapshot taken just before the transition occurs, finds a saddle point (TS2) where the H atom is located between the two O atoms (O···H···O angle of 171.1°) at a distance of 1.17 Å from the O of the NO_2 fragment and 1.32 Å from the O on the surface. The C′−O bond is not along the normal trajectory to the surface but is somewhat tilted, so that the three C−C′−O angles are 108.9, 108.1, and 92.2°. The normal mode with the imaginary frequency corresponds to the hopping of the H atom between the O atom on the graphite surface and the O atom belonging to the NO_2 fragment (see Supporting Information). The estimated barrier at 0 K is 4.4 kcal/mol. Such a small activation energy justifies the rather high formation rate of HONO in the atmosphere.

2.f. Other Electronic Energy Barriers. During the first metadynamics run we also observed the migration of the epoxide group on the surface. However, the CV selected for that run are not appropriate to estimate the energy barrier corresponding to the hops of the O atom on the surface. For such a simple

TABLE 3: Reaction Barriers (in kcal/mol) at Different Levels of Theory[a]

	MP2/G98	B3LYP/G98	BLYP/G98	BLYP/CPMD	
ethylene/6-311G**	54.0	53.1	41.9	38.8	ethylene/70 Ry
benzene/6-311G**		44.6	38.0		
benzene/6-311++G**		41.3	33.5	33.2	benzene/400 Ry

[a] The column on the left refers to the basis set employed in Gaussian 98, and the column on the right refers to the PW cutoff in CPMD. The TS of the reaction with benzene shows an important biradical character; therefore, we did use the NLCC and a high PW cutoff as explained previously.

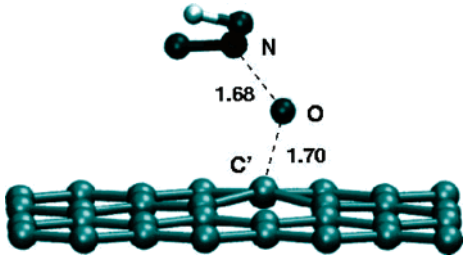

Figure 6. Geometry of the TS structure corresponding to the one-step epoxidation of the surface (TS4).

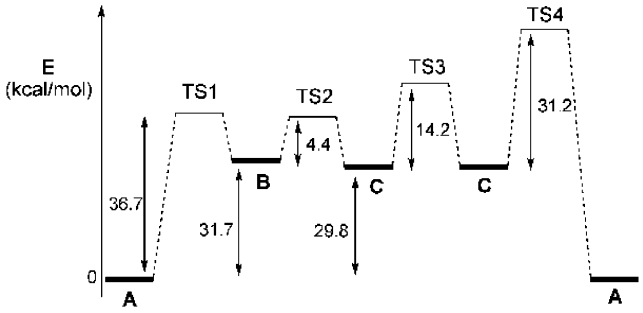

Figure 7. Energy profile for the minima and TS found for the oxidation of the graphite surface by means of HNO_3 and related processes after applying the metadynamics technique.

process the standard TS search can safely be used to determine the TS structure and the activation energy. As expected, in the TS (TS3), the O atom is bonded to only one C atom (Figure 3). The O−C′ bond distance is 1.43 Å; that is, it is smaller than in epoxidated or hydroxylated structures. Also, in this case, the C′ atom presents sp^3 hybridization. However, in contrast to what was observed for the optimized geometry of the hydroxylated surface, two of the C−C′−O angles are 100.7°, whereas the third is 106.8°. This difference is due to the fact that the C′−O bond is tilted toward the C atoms involved in the epoxide migration process. The average C−C′ distance is 1.50 Å. The normal model with the imaginary frequency corresponds to the displacement of the O atom over the surface from an epoxide position to another position (see Supporting Information). On the PES, the optimized transition structure is 14.2 kcal/mol higher in energy than the optimized epoxide.

We use a standard TS search also to analyze the TS of the oxidation by the one-step epoxidation process through the direct dissociation of a bare O atom from the nitric acid and its inverse reaction (process 5). The TS search is started from one high-energy configuration extracted from the reactive trajectory described in subsection 3.a (at about 9 ps) when the system is still in state C. The resulting TS (TS4) is shown in Figure 6.

The N···O distance is 1.68 Å, whereas C′···O is 1.70 Å. The N−O−C′ angle is 130.1°, that is, very far from linearity. Already at this stage the C′ atom undergoes a strong sp^3 hybridization and pyramidazilation with 1.47 Å being the average of the C′−C distances and 352.6° the sum of the three C−C′−C angles. The most important contributions to the normal mode with the imaginary frequency come from the formation and breakage of the N−O and C′−O bonds (see Supporting Information). The energy of TS4 is 31.2 kcal/mol higher than the energy of state C. This means that starting from A, we should expect an energy barrier of about 61 kcal/mol for the direct epoxidation. This makes this mechanism less probable than the two-step process of A to B to C (shown in Figure 7).

Conclusions

By making use of the new metadynamics method, we find that the interaction between the graphite surface and the nitric acid molecule is slightly repulsive in the absence of functionalities. Nevertheless, graphite can catalyze the dissociation of nitric acid if the partial gas pressure is such as to guarantee a high probability of having a HNO_3 molecule in the vicinity of the surface. The two possible products arising from the oxidation of the surface are the hydroxylated layer and the 1,2-epoxide structure. These two configurations are almost degenerate in energy despite their rather different electronic characters. The unpaired electron of the graphite−OH system is delocalized on the surface. The corresponding distribution of the spin density shows a regular pattern that distinguishes between odd and even neighbors of the C atom bonded to the OH group. From an analysis of the activation energies involved in the different processes observed, we conclude that the rate-limiting step in the oxidation is the first N−O bond breaking. The subsequent H transfer is, instead, very fast thanks to the rather low energy barrier, which explains the high rate of formation of nitrous acid in the atmosphere. By construction, the metadynamics algorithm gives access to all the available pathways, even those that cross higher TS and are, therefore, less probable. This is the case of the one-step dissociation mechanism described, where a bare O atom is directly transferred from the nitric acid to the graphite by breaking one of the stronger N−O bonds in the molecule.

Acknowledgment. The authors are grateful to Prof. J. Hutter, Dr. M. Krack, Dr. A. Laio, and F. Mohamed for fruitful discussions. A.R.-F. thanks the *Ministerio de Educación, Cultura y Deporte* (Spanish Government) for a postdoctoral fellowship.

Appendix

We have computed the reaction barriers for two gas-phase reactions involving HNO_3 and C−C bonds. For the reaction between nitric acid and ethylene, we have computed the barriers at MP2/6-311G** (geometries at B3LYP/6-311G** level), B3LYP/6-311G**, BLYP/6-311G**, and BLYP/PW levels. For the reaction between nitric acid and benzene, we have computed the barriers at B3LYP/6-311G**, BLYP/6-311G**, B3LYP/6-311++G**, and BLYP/6-311++G** (geometries at 6-311G** level). The results are shown in Table 3.

Supporting Information Available: Optimized geometries for the stationary points and normal modes of vibration with the imaginary frequency for each TS. This material is available free of charge via the Internet at http://pubs.acs.org.

References and Notes

(1) Albers, P. W.; Klein, H.; Lox, E. S.; Seibold, K.; Prescher, G.; Parker, S. F. *Phys. Chem. Chem. Phys.* **2000**, *2*, 1051.

(2) Buseck, P. R.; Posfai, M. *Proc. Natl. Acad. Sci. U.S.A.* **1999**, *96*, 3372.

(3) Palotás, A. B.; Rainey, L. C.; Sarofim, A. F.; Vander Sande, J. B.; Flagan, R. C. *CHEMTECH* **1998**, *July*, 24.

(4) Seinfeld, J. H.; Pandis, S. N. *Atmospheric Chemistry and Physics*; John Wiley & Sons: New York, 1998.

(5) Al-Abadleh, H. A.; Grassian, V. H. *J. Phys. Chem. A* **2000**, *104*, 11926.

(6) Choi, W.; Leu, M.-T. *J. Phys. Chem. A* **1998**, *102*, 7618.

(7) Gerecke, A.; Thielmann, A.; Gutzwiller, L.; Rossi, M. *Geophys. Res. Lett.* **1998**, *25*, 2453.

(8) Hauglustaine, D. A.; Ridley, D. A.; Solomon, S.; Hess, P. G.; Madronich, S. *Geophys. Res. Lett.* **1996**, *23*, 2609.

(9) Kirchner, U.; Scheer, V.; Vogt, R. *J. Phys. Chem. A* **2000**, *104*, 8908.

(10) Kleffmann, J.; Becker, K.; Lackhoff, M.; Wiesen, P. *Phys. Chem. Chem. Phys.* **1999**, *1*, 5443.

(11) Lary, D. J.; Lee, A. M.; Toumi, R.; Newchurch, M. J.; Pirre, M. J.; Renard, J. B. *J. Geophys. Res.* **1997**, *102*, 3671.

(12) Longfellow, C. A.; Ravishankara, A. R.; Hanson, D. R. *J. Geophys. Res.* **1999**, *104*, 13833.

(13) Ravishankara, A. R. *Science* **1997**, *276*, 1058.

(14) Rogaski, C. A.; Golden, D. M.; Williams, D. L. *Geophys. Res. Lett.* **1997**, *24*, 381.

(15) Bekki, S. J. *J. Geophys. Res.* **1997**, *102*, 10751.

(16) Chatfield, R. B. *Geophys. Res. Lett.* **1994**, *21*, 2705.

(17) Lammel, G.; Novakov, T. *Atmos. Environ.* **1995**, *29*, 813.

(18) Collignon, B.; Hoang, P. N. M.; Picaud, S.; Rayez, J. C. *Chem. Phys. Lett.* **2005**, *406*, 430.

(19) Fuente, E.; Menéndez, J. A.; Díez, M. A.; Suárez, D.; Montes-Morán, M. A. *J. Phys. Chem. B* **2003**, *107*, 6350.

(20) Ghigo, G.; Maranzana, A.; Tonachini, G.; Zicovich-Wilson, C. M.; Causà, M. *J. Phys. Chem. B* **2004**, *108*, 3215.

(21) Hamad, S.; Mejias, J. A.; Lago, S.; Picaud, S.; Hoang, P. N. M. *J. Phys. Chem. B* **2004**, *108*, 5405.

(22) Montoya, A.; Truong, T. N.; Sarofim, A. F. *J. Phys. Chem. A* **2000**, *104*, 6108.

(23) Picaud, S.; Hoang, P. N. M.; Hamad, S.; Mejias, J. A.; Lago, S. *J. Phys. Chem. B* **2004**, *108*, 5410.

(24) Tarasevich, Y. I.; Aksenenko, E. V. *Colloids Surf., A* **2003**, *215*, 285.

(25) Zhu, Z.; Lu, G. Q.; Finnerty, J.; Yang, R. T. *Carbon* **2003**, *41*, 635.

(26) Pierson, H. O. *Handbook of Carbon, Graphite, Diamond and Fullerenes - Properties, Processing and Applications*; William Andrew Publishing/Noyes: Norwich, NY, 1993.

(27) Iannuzzi, M.; Laio, A.; Parrinello, M. *Phys. Rev. Lett.* **2003**, *90*, 238302.

(28) Laio, A.; Parrinello, M. *Proc. Natl. Acad. Sci. U.S.A.* **2002**, *99*, 12562.

(29) Boero, M.; Ikeshoji, T.; Liew, C. C.; Terakura, K.; Parrinello, M. *J. Am. Chem. Soc.* **2004**, *126*, 6280.

(30) Churakov, S. V.; Iannuzzi, M.; Parrinello, M. *J. Phys. Chem. B* **2004**, *108*, 11567.

(31) Gervasio, F. L.; Laio, A.; Iannuzzi, M.; Parrinello, M. *Chem.—Eur. J.* **2004**, *10*, 4846.

(32) Iannuzzi, M.; Parrinello, M. *Phys. Rev. Lett.* **2004**, *93*, 025901.

(33) Stirling, A.; Iannuzzi, M.; Laio, A.; Parrinello, M. *ChemPhysChem* **2004**, *5*, 1558.

(34) *CPMD*, version 3.7; IBM Corp.: White Plains, NY, 1990−2001 (Copyright MPI für Festkörperforschung Stuttgart 1997−2001).

(35) Car, R.; Parrinello, M. *Phys. Rev. Lett.* **1985**, *55*, 2471.

(36) Becke, A. *Phys. Rev. A: At., Mol., Opt. Phys.* **1988**, *38*, 3098.

(37) Lee, C.; Yang, W.; Parr, R. *Phys. Rev. B: Condens. Matter* **1988**, *37*, 785.

(38) Troullier, N.; Martins, J. L. *Phys. Rev. B: Condens. Matter* **1991**, *43*, 1993.

(39) Billeter, S. R.; Curioni, A.; Andreoni, W. *Comput. Mater. Sci.* **2003**, *27*, 437.

(40) Liu, D. C.; Nocedal, J. *Math. Prog.* **1989**, *45*, 503.

(41) Frisch, M. J.; Trucks, G. W.; Schlegel, H. B.; Scuseria, G. E.; Robb, M. A.; Cheeseman, J. R.; Zakrzewski, V. G.; Montgomery, J. A., Jr.; Stratmann, R. E.; Burant, J. C.; Dapprich, S.; Millam, J. M.; Daniels, A. D.; Kudin, K. N.; Strain, M. C.; Farkas, O.; Tomasi, J.; Barone, V.; Cossi, M.; Cammi, R.; Mennucci, B.; Pomelli, C.; Adamo, C.; Clifford, S.; Ochterski, J.; Petersson, G. A.; Ayala, P. Y.; Cui, Q.; Morokuma, K.; Malick, D. K.; Rabuck, A. D.; Raghavachari, K.; Foresman, J. B.; Cioslowski, J.; Ortiz, J. V.; Stefanov, B. B.; Liu, G.; Liashenko, A.; Piskorz, P.; Komaromi, I.; Gomperts, R.; Martin, R. L.; Fox, D. J.; Keith, T.; Al-Laham, M. A.; Peng, C. Y.; Nanayakkara, A.; Gonzalez, C.; Challacombe, M.; Gill, P. M. W.; Johnson, B. G.; Chen, W.; Wong, M. W.; Andres, J. L.; Head-Gordon, M.; Replogle, E. S.; Pople, J. A. *Gaussian 98*, revision A.11; Gaussian, Inc.: Pittsburgh, PA, 1998.

(42) Kristyán, S.; Pulay, P. *Chem. Phys. Lett.* **1994**, *229*, 175.

(43) Meijer, E. J.; Sprik, M. *J. Chem. Phys.* **1996**, *105*, 8684.

(44) Pérez-Jordá, J. M.; Becke, A. *Chem. Phys. Lett.* **1995**, *233*, 134.

(45) Sprik, M. *Faraday Discuss.* **1998**, *110*, 437.

(46) Chase, M. W., Jr.; Davles, C. A.; Downey, J. R., Jr.; Frurip, D. J.; McDonald, R. A.; Syverud, A. N. *J. Phys. Chem. Ref. Data* **1985**, *14* (Suppl. 1), 1.

(47) Chakraborty, D.; Park, J.; Lin, M. C. *Chem. Phys.* **1998**, *231*, 39.

(48) Donahue, N. M.; Dubey, M. K.; Morhschladt, R.; Demerjian, K. L.; Anderson, J. G. *J. Geophys. Res.* **1997**, *102*, 6159.

(49) Tsang, W.; Herron, J. T. *J. Phys. Chem. Ref. Data* **1991**, *20*, 609.

(50) Doclo, K.; Röthlisberger, U. *Chem. Phys. Lett.* **1998**, *297*, 205.

(51) Houk, K. N.; Condroski, K. R.; Pryor, W. *J. Am. Chem. Soc.* **1996**, *118*, 13002.

(52) Sumathi, R.; Peyerhimhoff, S. D. *J. Chem. Phys.* **1997**, *107*, 1872.

(53) Louie, S. G.; Froyen, S.; Cohen, M. L. *Phys. Rev. B: Condens. Matter* **1982**, *26*, 1738.

(54) Engel, E.; Höck, A.; Schmid, R. N.; Dreizler, R. M.; Chetty, N. *Phys. Rev. B: Condens. Matter* **2001**, *64*, 125111.

(55) Porezag, D.; Pederson, M. R.; Liu, A. Y. *Phys. Rev. B: Condens. Matter* **1999**, *60*, 14132.

(56) Goldstein, E.; Beno, B.; Houk, K. N. *J. Am. Chem. Soc.* **1996**, *118*, 6036.

(57) Houk, K. N.; Beno, B. E.; Nendel, M.; Black, K.; Yoo, H. Y.; Wilsey, S.; Lee, J. K. *THEOCHEM* **1997**, *398−399*, 169.

(58) Hrovat, D. A.; Beno, B. R.; Lange, H.; Yoo, H. Y.; Houk, K. N.; Borden, W. T. *J. Am. Chem. Soc.* **2000**, *122*, 7456.

(59) Ozkan, I.; Kinal, A. *J. Org. Chem.* **2004**, *69*, 5390.

(60) Elstner, M.; Hobza, P.; Fruenheim, T.; Suhai, S.; Kaxiras, E. *J. Chem. Phys.* **2001**, *114*, 5149.

(61) Wu, Q.; Yang, W. *J. Chem. Phys.* **2002**, *116*, 515.

(62) Wu, X.; Vargas, M. C.; Nayak, S.; Lotrich, V.; Scoles, G. *J. Chem. Phys.* **2001**, *115*, 8748.

(63) Zimmerli, U.; Parrinello, M.; Koumoutsakos, P. *J. Chem. Phys.* **2004**, *120*, 2693.

(64) Cox, A. P.; Ellis, M. C.; Attfield, C. J.; Ferris, A. C. *J. Mol. Struct.* **1994**, *320*, 91.

(65) The parameters used in the extended Lagrangian scheme of this metadynamics are the following: $k_1 = 0.8$ au, $M_1 = 10$ amu, $k_2 = 0.8$ au, $M_2 = 10$ amu, $k_3 = 0.8$ au, and $M_3 = 10$ amu. The average height of the hills (W_{av}) is 6.6 kcal/mol, their perpendicular width ($\Delta s^{\perp}$) is 0.4, and the deposition rate (Δt) is 0.006 ps.

(66) Lerf, A.; He, H.; Forster, M.; Klinowski, J. *J. Phys. Chem. B* **1998**, *102*, 4477.

(67) Chen, N.; Yang, R. T. *J. Phys. Chem. A* **1998**, *102*, 6348.

(68) Sorescu, D. C.; Jordan, K. D.; Avouris, P. *J. Phys. Chem. B* **2001**, *105*, 11227.

(69) Cano, J.; Ruiz, E.; Alvarez, S.; Verdaguer, M. *Comments Inorg. Chem.* **1998**, *20*, 27.

(70) Ruiz, E.; Rodríguez-Fortea, A.; Alvarez, S. *Inorg. Chem.* **2003**, *42*, 4881.

(71) The parameters used in this metadynamics are the following: $k_1 = 0.6$ au, $M_1 = 15$ amu, $k_2 = 0.6$ au, $M_2 = 15$ amu, $k_3 = 0.6$ au, and $M_3 = 15$ amu. $W_{av} = 1.0$ kcal/mol, $\Delta s^{\perp} = 0.06$, and $\Delta t = 0.009$ ps. The values used for the cutoff distances are $d_{NO} = d_{NC} = d_{OC} = 1.64$ Å.

(72) Jenkin, M. E.; Cox, R. A.; Williams, D. J. *Atmos. Environ.* **1988**, *22*, 487.

(73) Stadler, D.; Rossi, M. J. *Phys. Chem. Chem. Phys.* **2000**, *2*, 5420.

(74) Tabor, K.; Gutzwiller, L.; Rossi, M. J. *J. Phys. Chem.* **1994**, *98*, 6172.